Published in final edited form as:

Nat Biotechnol. 2018 January ; 36(1): 103–112. doi:10.1038/nbt.4024.

Global landscape of cell envelope protein complexes in *Escherichia coli*

Mohan Babu[1,15,16], **Cedoljub Bundalovic-Torma**[2,3,15], **Charles Calmettes**[3,4,15], **Sadhna Phanse**[1,5], **Qingzhou Zhang**[1], **Yue Jiang**[2], **Zoran Minic**[1], **Sunyoung Kim**[1], **Jitender Mehla**[6], **Alla Gagarinova**[7], **Irina Rodionova**[8], **Ashwani Kumar**[9], **Hongbo Guo**[5], **Olga Kagan**[5], **Oxana Pogoutse**[5], **Hiroyuki Aoki**[1], **Viktor Deineko**[1], **J Harry Caufield**[6], **Erik Holtzapple**[7,8], **Zhongge Zhang**[8], **Ake Vastermark**[8], **Yogee Pandya**[5], **Christine Chieh-lin Lai**[3], **Majida El Bakkouri**[3], **Yogesh Hooda**[3], **Megha Shah**[3], **Dan Burnside**[10], **Mohsen Hooshyar**[10], **James Vlasblom**[1], **Sessandra V Rajagopala**[11], **Ashkan Golshani**[10], **Stefan Wuchty**[12], **Jack F Greenblatt**[5,13], **Milton Saier**[8,16], **Peter Uetz**[6,16], **Trevor F Moraes**[3,16], **John Parkinson**[2,3,13,16], and **Andrew Emili**[5,13,14,16]

[1]Department of Biochemistry, University of Regina, Regina, Saskatchewan, Canada

[2]Hospital for Sick Children, Toronto, Ontario, Canada

[3]Department of Biochemistry, University of Toronto, Toronto, Ontario, Canada

[4]INRS-Institut Armand Frappier, Laval, Québec, Canada

[5]Donnelly Centre, University of Toronto, Toronto, Ontario, Canada

[6]Virginia Commonwealth University, Richmond, Virginia, USA

[7]Department of Biochemistry, University of Saskatchewan, Saskatoon, Canada

[8]Department of Molecular Biology, UC San Diego, La Jolla, California, USA

[9]Department of Computer Science, University of Regina, Regina, Saskatchewan, Canada

[10]Department of Biology, Carleton University, Ottawa, Ontario, Canada

[11]J. Craig Venter Institute, Rockville, Maryland, USA

[12]Department of Computer Science and Department of Biology, University of Miami, Coral Gables, Florida, USA

Correspondence should be addressed to A.E. (aemili@bu.edu) or M.B. (mohan.babu@uregina.ca).
[15]These authors contributed equally to this work.
[16]These authors jointly supervised this work.

AUTHOR CONTRIBUTIONS

M.B. and A.E. designed and together supervised the project. Y.P. and O.P. constructed tagged strains. O.K., S.K. and V.D. performed protein purifications, while H.G. and Z.M. performed MS analyses. S.P. performed database searches and curation, and created the web portal. C.C., S.K., J.M., V.K., I.R., A.Ga., H.A., E.H., Z.Z., A.V., D.B., M.H., C.C.L., M.E.B., Y.H., M.S. and S.V.R. performed the follow-up and validation experiments. C.B.-T., S.P., Q.Z., Y.J., A.K., J.H.C. and S.W. performed the scoring and data analysis. M.B. and A.E. wrote the manuscript, with input from C.B.-T., C.C., J.V., A.Go., J.F.G., M.S., P.U., T.F.M. and J.P. All authors read and approved the manuscript.

COMPETING FINANCIAL INTERESTS

The authors declare no competing financial interests.

Note: Any Supplementary Information and Source Data files are available in the online version of the paper.

[13]Department of Molecular Genetics, University of Toronto, Toronto, Ontario, Canada

[14]Department of Biology and Biochemistry, Boston University, Boston, Massachusetts, USA

Abstract

Bacterial cell envelope protein (CEP) complexes mediate a range of processes, including membrane assembly, antibiotic resistance and metabolic coordination. However, only limited characterization of relevant macromolecules has been reported to date. Here we present a proteomic survey of 1,347 CEPs encompassing 90% inner- and outer-membrane and periplasmic proteins of *Escherichia coli*. After extraction with non-denaturing detergents, we affinity-purified 785 endogenously tagged CEPs and identified stably associated polypeptides by precision mass spectrometry. The resulting high-quality physical interaction network, comprising 77% of targeted CEPs, revealed many previously uncharacterized heteromeric complexes. We found that the secretion of autotransporters requires translocation and the assembly module TamB to nucleate proper folding from periplasm to cell surface through a cooperative mechanism involving the β-barrel assembly machinery. We also establish that an ABC transporter of unknown function, YadH, together with the Mla system preserves outer membrane lipid asymmetry. This *E. coli* CEP 'interactome' provides insights into the functional landscape governing CE systems essential to bacterial growth, metabolism and drug resistance.

As in eukaryotes such as yeast[1], an extensive, but still largely unknown, network of physical associations mediates the diverse and vital roles of CEPs in bacterial membrane biology, pathogenesis and antibiotic resistance[2,3]. Knowledge of cell envelope protein–protein interactions (cePPIs) and their physical and functional organization into multiprotein complexes (MPCs) therefore provides critical information into the basic systems governing prokaryotic physiology, which in turn is essential to combat infections by antibiotic-resistant pathogens. Yet while previous small-scale investigations in *E. coli* have identified certain MPCs required for peptidoglycan synthesis, chemotaxis, lipopolysaccharide (LPS) export and envelope assembly[2,4,5], experimental data concerning the binding partners and functions of most bacterial CEPs are still lacking[6].

To address this important gap, we performed large-scale affinity-tagging for hundreds of engineered *E. coli* CE strains bearing C-terminal sequential peptide affinity (SPA) chromosomal tags to maintain cognate promoter regulation and physiologic expression levels[7,8]. We then purified these SPA-tagged fusion proteins under non-denaturing conditions and analyzed them by mass spectrometry (MS) to elucidate the compositions of native CE-associated macromolecular assemblies. The resulting high-confidence physical interaction map substantially extends knowledge of the CE interactome, and complements our previous characterization of soluble cytoplasmic protein complexes in *E. coli*[7,8].

RESULTS

Generating a high-quality CEP interaction data set

Most CEPs are not readily solubilized using the standard combination of affinity purification and MS (AP/MS) workflow we developed to isolate soluble protein complexes[7,8]. To

facilitate extraction of hydrophobic assemblies[1,6] we used non-denaturing detergent solubilization procedures adapted from our previous study of yeast MPCs[1]. After evaluating 14 diverse detergents (1% w/v or v/v; Supplementary Fig. 1a–c), we selected $C_{12}E_8$ (octaethylene glycol monododecyl ether), DDM (n-dodecyl-d-maltoside) and Triton X-100 (octylphenol ethoxylate) as the most effective non-ionic detergents for recovery of diverse endogenous SPA-tagged MPCs from late log-phase *E. coli* (DY330) cultures grown in rich media (Supplementary Note 1).

Based on current subcellular annotations available in public databases, as well as widely used prediction programs, literature curation, and other information sources (Supplementary Note 1), we compiled a list of 1,617 annotated or predicted CEPs. Of these, we attempted to create chromosomal SPA-fusions for 1,347 proteins (Supplementary Table 1), whereas the remaining were not targeted due to questionable 'legacy' annotations. In total, we tagged over half (58%, 785 of 1,347) of the CEPs that were confirmed by immunoblotting or PCR; the remaining (562) were not detected under standard culture conditions, but a sizeable (41%; 229) fraction were subsequently identified as co-purifying interactors with the successful bait purifications.

From our proteome-wide analysis, in total, we successfully purified 785 CEPs (Fig. 1a and Supplementary Table 1), many of which (88%, 693 CEPs) have been associated with drug sensitivity and the intrinsic antibiotic 'resistome'[9] (Supplementary Fig. 1d). These include 549 inner membrane proteins (IMPs), 45 outer membrane proteins (OMPs), and 129 periplasmic proteins (PEPs) involved in diverse processes encompassing transport, CE assembly and biofilm formation; 45 lipoproteins (6 IM, 39 OM); 15 extracellular space proteins; and two putative membrane-related proteins[6,10].

To evaluate data quality and reproducibility, we affinity-purified 290 SPA-tagged CEPs using one to three different detergents, with multiple biological replicates per detergent, for a total of 1,751 AP/ MS analyses (Supplementary Note 1). The remaining 495 baits were subject to AP/MS once, in the presence of 1 to 3 different detergents, for an additional 1,103 analyses (Supplementary Fig. 2a). In total, 2,854 affinity-purified CEP samples were analyzed by Orbitrap MS. CEP recovery (coverage) was consistently high regardless of protein topology (68% IMPs, 79% OMPs, 86% PEPs; Supplementary Fig. 2b), but was influenced by protein abundance (Supplementary Fig. 2c) and the number of predicted transmembrane helices or β-strands (Supplementary Fig. 2d). We successfully recovered most (84%, 147 of 175 tagged) CEP harboring annotated Pfam domains (Supplementary Fig. 2e), including ATP-binding cassette (ABC), 4Fe-4S ferredoxin and polypeptide transport associated (POTRA) domain-containing proteins (e.g., BamA), which are under-represented in public PPI databases. The average correlation between replicates (calculated based on protein spectral counts detected by MS) was high ($r = 0.7$), with low ($\sigma = 0.1$) variance (Fig. 1b), indicating the overall reproducibility, which is comparable to previous AP/MS-based analyses of soluble protein interaction networks[11,12].

Interaction scoring and benchmarking

To derive a high-fidelity CE network, we mapped the MS/MS spectra obtained from each SPA-tagged bait purification to reference *E. coli* protein sequences using both the

SEQUEST/ STATQUEST[8] and alternate MS-GF+[13] algorithms to boost peptide identification (Supplementary Note 1). The PPI data from each bait CEP were then filtered using a protein identification probability score of 90% or greater. The cut-off was chosen because the majority of known interactions curated in EcoCyc (a comprehensive database resource for *E. coli*) passed this threshold (Supplementary Fig. 3a), eliminating promiscuous non-specific interactors and retaining reliable interactions with adequate specificity. These filtered associations were then subjected to an integrative statistical framework to computationally assign interaction confidence scores (Supplementary Note 1), and we benchmarked the results against reference cePPIs curated in EcoCyc. We maximized coverage and accuracy using Bayesian inference[14] to normalize and integrate the output of CompPASS (Comparative Proteomic Analysis Software Suite)[15] and HGSCore (HyperGeometric Spectral Counts score)[16] algorithms into a single unified probabilistic log-likelihood score (LLS) for each putatively interacting bait–prey and prey–prey protein pair (Fig. 1c and Supplementary Fig. 3b).

We eliminated associations below a stringent integrated score threshold (Σ LLS $\leq$ 5.27) that faithfully recapitulated known (positive reference) cePPIs according to area-under-the ROC (receiver operating characteristic) curve analysis (Fig. 1c and Supplementary Table 2). The final probabilistic network consists of 12,801 putative interactions and includes 77% (604) of all targeted *E. coli* CEPs (Supplementary Table 2), with broad representation across protein size, topology and function. Notably, despite ample anecdotal supporting evidence (Supplementary Table 3 and Supplementary Note 2), most (12,523) of these physical interactions, and one-quarter (217) of the CEPs have not been detected before[8,17–19] (Fig. 1d). Similar to yeast[1], each *E. coli* CEP had slightly fewer interaction partners by AP/MS than soluble proteins[8] ($P = 4.2 \times 10^{-10}$; Supplementary Fig. 3c), possibly due to detergent-mediated disruption of lower abundance or weaker binding partners.

Network validation

Multiple criteria support the overall reliability of network and underlying AP/MS data. We categorized interactions as one of two types (Supplementary Table 2): high-confidence (HC), representing half (46%, or 5,927) of the cePPIs, which were reproducibly detected by multiple replicates, different detergents, alternate methods (yeast and/ or bacterial two-hybrid assays or biochemical fractionation coupled to MS; see below), or reported in a previous interaction study[7,8,19]; and medium-confidence (MC; 53%, 6,770) that are predicted to have a functional-association by STRING[20], GeneMANIA[21], or genomic context[8], or which co-localize to the same compartment (Fig. 1e).

While the few remaining (<1%, 104) prey–prey associations were among cytoplasmic protein pairs, we also gained meaningful functional insights from these subnetworks into membrane transport metabolons (i.e., physical coupling of transporters and enzymes; see below) and other pathways[22] (Fig. 1e and Supplementary Note 1).

When benchmarked against manually curated MPCs (Fig. 1f), both the high and medium confidence cePPIs recapitulated annotated assemblies more faithfully (e.g., average semantic similarity[23]) than previously published large-scale[8,18,19] and small-scale *E. coli* studies[17] (Supplementary Fig. 3d). As expected for functional macromolecules, genes encoding

putatively interacting CEPs also had more similar genetic interaction patterns[10,24,25] (Supplementary Fig. 3e) and drug sensitivity profiles[9] (Supplementary Fig. 3f and Supplementary Table 3) as compared to random gene pairs, indicating enrichment for physiologically relevant associations. We note that one-third (30%, 3,853) of the total number (12,801) of protein pairs derived from the HGSCore algorithm were “prey–prey” associations (i.e., co-purifying non-bait interactors; Fig. 1e), most (3,710) of which are medium confidence and involve at least one CEP. Nevertheless, these interactions are functionally informative; for example, the high and/or medium confidence cePPIs both showed high sensitivity and reasonable specificity (based on fivefold cross-validation) as compared to previously published *E. coli* PPI data sets[8,18,19] (Supplementary Fig. 3g).

To independently verify the global reliability of the AP/MS results, we employed a complementary proteomic approach to detect endogenous (untagged) macromolecules based on co-fractionation during size-exclusion chromatography of detergent-solubilized (0.020% Triton and 0.05% DDM) *E. coli* extracts (Supplementary Fig. 4a and Supplementary Note 1). As with previous soluble protein complexes[26,27], we used quantitative MS to compare the co-elution profiles of proteins across the collected fractions (Supplementary Fig. 4b). From these we computed interaction likelihood metrics (Supplementary Note 1), which we then benchmarked against the EcoCyc reference set (Supplementary Fig. 4c). Co-purifying protein pairs showing high similarity ($r = 0.8$; Supplementary Fig. 4d) recapitulated an additional 13% (1,678) of the putative candidate cePPIs detected by AP/MS (Supplementary Table 2), providing further evidence of a stable native biophysical association.

We next subjected a subset of cePPIs to further independent experimental evaluation based on binary yeast and/or bacterial two-hybrid assays (Supplementary Note 1). Of the 103 pairs randomly selected from high confidence (81) and medium confidence (22) cePPI categories, we confirmed almost half (44, or 43%; Supplementary Fig. 4e and Supplementary Table 3), which agrees favorably with the validation rates obtained from analogous assays for *E. coli* soluble PPIs[19]. Confirmed association pairs include the putative fimbrial adhesion protein YehA with the periplasmic chaperone YehC, representing a putative chaperone-usher assembly pathway required for pilus/fimbrium biogenesis and biofilm formation, and the OM channel CusC and the membrane fusion protein CusB, representing a physical coupling underlying the copper/silver efflux system.

Topological properties of the MPC network

We examined the global topological organization of the cePPI network in comparison to the *E. coli* cytoplasmic interactome[7,8]. As seen for soluble protein complexes[8], we found that essential CEPs (59, 4.4%), many of which (18) are targeted by antibiotics[9] (Supplementary Fig. 5a), had higher connectivity than non-essential CEPs ($P = 4.5 \times 10^{-7}$; Supplementary Fig. 5b), as did evolutionarily conserved CEPs (Supplementary Fig. 5c), particularly peptidoglycan and cell wall proteins, whereas extracellular proteins tended to have the fewest partners (Supplementary Fig. 5d).

Half (46%, 5,939) of the interacting proteins co-localized to the same compartment, while many other PPIs (54%, 6,862; $P = 4.2 \times 10^{-2}$) bridged the Gram-negative CE compartments, of which three-fourths (79%, 5,451) occurred between CEPs and cytosolic proteins

(Supplementary Fig. 5e and Supplementary Table 2). The latter include links between the IM Sec translocon (SecDEY) and cytosolic proteases (ClpAPX) involved in degradation and folding, suggesting bacterial protein homeostasis is coupled to protein translocation[28] (Supplementary Note 2). Similarly, interactions between the periplasmic hydrogenase 2 small subunit (HybO) and cytoplasmic fumarate reductase (FrdB) suggest coordination in substrate reduction (such as quinones) during anaerobic respiration[29]. The β-barrel assembly OMP (BamA) and OM lipoproteins (BamCDE) also co-purified with the IM Sec translocon (SecDFGY), consistent with a primary role in β-barrel translocation, transport and membrane insertion OMP biogenesis[30].

To define complex membership, we partitioned the cePPI network (high + medium confidence) into densely connected regions using a 'core-attachment' clustering algorithm[31]. In total, we identified 540 MPCs, of which 420 contain at least one CEP and 120 involve only cytosolic proteins (Fig. 2 and Supplementary Table 4), with predicted topologies consisting of either 54 matrix (i.e., interaction among all components), 68 spoke (i.e., bait connectivity with prey proteins), and 123 socio-affinity (i.e., integration of spoke and matrix) models based on the degree of PPI connectivity (the remaining 295 complexes were either binary or involve prey–prey associations). These clusters encompass 246 heterodimers (Supplementary Fig. 6a), of which over half (252, 60%) matched known (EcoCyc curated) assemblies (Supplementary Fig. 6b), while one-quarter (103, 25%) were bridged by cePPIs (88; as determined by bacterial or yeast two-hybrid assay; Supplementary Fig. 6c). The remaining 168 CEP complexes have not been reported before (Supplementary Table 4), representing a rich resource for biological discovery.

Membrane-associated metabolons

Several of the MPCs represent potential membrane transport metabolons[32] encompassing sugar permeases, components of the phosphoenolpyruvate-dependent phosphotransferase system (PTS), and the histidine-containing phosphocarrier energy coupling protein (HPr or PtsH; Supplementary Table 3). HPr and other soluble energy-coupling proteins (e.g., sugar-specific IIA proteins) are known to associate with PTS permeases[32], and our data link different transport complexes of the PTS. For instance, fructose PTS permease (FruA) co-purified with enzyme IIC constituents (e.g., GatC, NagE, TreB, MngA) in addition to its cognate energy-coupling factor, FruB[33]. Although not strictly membrane-bound[22], HPr also co-purified with multiple regulatory targets (e.g., Adk, DhaK, PfkB, PykF; Supplementary Note 2). HPr is known to bind pyruvate kinase A (PykA) in the opportunistic pathogen *Vibrio vulnificus*[34], whereas *E. coli* HPr interacts with an isozyme, pyruvate kinase 1 (PykF). We confirmed the latter association by steady-state kinetics (Supplementary Fig. 7a), and found that PykF is activated upon binding to non-phosphorylated HPr, suggesting that, similar to PykA[34] of *V. vulnificus*, HPr regulates PykF by increasing its affinity for phosphoenolpyruvate.

Other interactions indicative of transporter-based metabolons (Supplementary Fig. 7b and Supplementary Note 2) include the housekeeping dipeptide permease Dpp, which co-purified with heterodimeric ATPases (DppDF) IMPs (DppBC) and the periplasmic peptide-binding protein DppA of the ABC peptide uptake system (Supplementary Fig. 7c),

consistent with joint participation in peptide transport[35]. Likewise, the zinc transporter ZnuA co-purified with the PEP ZinT (YodA), and a zinc-uptake ABC transporter composed of the membrane permease ZnuB and the ATPase ZnuC[36] (Supplementary Fig. 7d). It has been proposed that ZinT cooperates with ZnuA in zinc periplasmic uptake[36], although its role in zinc homeostasis is not clear. Interaction of ZnuA with the transcriptional regulator MntR points to a possible control mechanism[37], and the association of ZinT/ZnuA with the periplasmic receptor AraF (of the arabinose ABC transporter AraFGH; Supplementary Fig. 7d) implies metabolic coupling. The periplasmic receptor AraF that binds l-arabinose in the periplasm and delivers it to the IMP complex AraGH[38] was also consistent with the physical link we observed. Similarly, multiple polycistronic operons, wherein a substrate-producing enzyme is co-expressed with a cognate transporter[32], exhibited high physical connectivity (Supplementary Fig. 7e).

MPCs linked to antibiotic susceptibility

Defects in envelope assembly often disrupt the cell permeability barrier, leading to drug hypersensitivity[9]. We therefore examined the cePPI/MPC network for links to antibiotic susceptibility. A significant enrichment ($P \leq 0.05$) for drug hypersensitivity was evident among *E. coli* strains lacking components of 68 MPCs (Fig. 3a and Supplementary Table 5), indicating a critical role in envelope integrity. These include mutants of core-oligosaccharide assembly factor *waa* (formerly *rfa*), which are hypersensitive to numerous antimicrobials[9], presenting an attractive target for antibiotic potentiation. Mutations in components of the Tol-Pal envelope (*tolBQ*, *pal*) and purine (*purDHLMT*) systems also confer hypersensitivity to similar inhibitors[9], consistent with overlapping cellular roles.

Because multidrug resistance (MDR) is a major emerging clinical concern[39], we assessed the association of the multidrug transporter MdtF (YhiV) with a periplasmic lipoprotein (AcrA) of the AcrAB-TolC efflux pump (Supplementary Table 2). We found that if either *mdtF* or *acrA* was expressed alone (in an *acrAB mdtEF* quadruple mutant), export of an efflux test substrate (ethidium bromide) or antibiotics (levofloxacin, carbenicillin) was impaired. However, when *acrA* is co-expressed with *mdtF*, substantial transport of substrate antibiotics was observed (Fig. 3b), to a similar extent as upon coexpression of MdtE and MdtF (which are known to interact), consistent with AcrA and MdtF associating to form a functional drug efflux pump.

Bam-Tam interplay

Another notable MPC had unexpected connections between a membrane-spanning translocation and assembly module (Tam) with the OMP biogenesis (BAM) machinery (Fig. 4a). TamA and TamB have been implicated in autotransporter secretion[40], which is consistent with the interaction observed with an autotransporter processing protein (Ag43), but their precise role in Type V secretion is unclear (Supplementary Note 2). Whereas TamA, an OMP of the Omp85 family and a BamA homolog[41], consisting of an N-terminal periplasmic domain composed of three POTRA repeats preceding a 16-stranded C-terminal β-barrel (Supplementary Fig. 8a), is restricted to Proteobacteria and Bacteroidetes[41], TamB, an IMP with an N-terminal transmembrane helix, a C-terminal DUF490 domain (crucial for envelope integrity), and a large inter-domain with no assigned function, is widespread

among Gram-negative bacteria[42]. Of note, we found that loss of either *tamA* or *tamB* enhanced the slow growth phenotype of *E. coli* mutants lacking *bamA* (Supplementary Note 2) but not other *bam* components of the BAM export system (Fig. 4b), suggesting involvement in BamA-mediated export, the dominant secretion mechanism for Type V autotransporters.

To examine this, we performed agglutination assays (Fig. 4c). Notably, *tamB* but not *tamA* mutants had impaired autotransporter secretion (Ag43 (Flu), AidA and TibA (Type Va), YadA (Type Vc)), and sedimentation profiles similar to that of control cells not expressing any autotransporters (Fig. 4d). The translocation of the N-terminal passenger domain of Ag43 to the outer cell surface, assessed by both flow cytometry (Fig. 4e,f) and transmission electron microscopy (Supplementary Fig. 8b), was normal in *tamB* mutants, but folding was deficient (Fig. 4g; Ag43 shown). This is evident because Ag43 autotransporters are far more sensitive to proteinase K treatment in *tamB* knockouts (complete digestion after 1 h) as compared to wild-type cells, which is indicative of misfolding of Ag43 in the absence of TamB (Supplementary Note 2).

To exclude a translocation defect, we monitored Ag43 secretion based on thermal release of the processed N-terminal passenger domain, which is proteolytically cleaved (after amino acid D551 by an unidentified protease) and detached by heat denaturation (60 °C)[43]. As in wild-type cells, the mature N-terminal passenger domain completely disappeared from the cell surface of heat-shocked *tamB* mutants, as shown by flow cytometry (Fig. 4e,f), while the released αAg43 fragment was detected in the culture supernatant (Supplementary Fig. 8c–e). This leads to a working model (Fig. 4h and Supplementary Note 2) in which BamA-TamA/B function together during TamB-nucleated folding of the mature N-terminal passenger domain, catalyzing β-domain membrane insertion to facilitate translocation of partially folded autotransporters.

Transporter complex confers lipid asymmetry

Another notable MPC consisted of an IM ABC transporter of unknown function, YadH, in association with four (of six) subunits of a broadly conserved Mla-family phospholipid transporter (composed of the OM lipoprotein MlaA, a substrate-binding IMP MlaD, the cytosolic STAS domain protein MlaB, and a nucleotide-binding IMP MlaF) that maintains OM lipid asymmetry[44] (Fig. 5a). Consistent with joint participation in phospholipid transport, we verified these interactions by bacterial two-hybrid and repeat AP/MS experiments (Fig. 5b). Functionally, we found that *yadH* null cells were as hypersensitive as *mlaA* mutants to reagents like SDS/EDTA that destabilize LPS, causing phospholipid buildup in the OM[44] (Fig. 5c). This hyperpermeability phenotype was not enhanced in *yadH mla* double mutants (Fig. 5c), consistent with a cooperative function, and was suppressed by overexpressing the phospholipase *pldA*, which targets surface-exposed phospholipid. As with *mla*[44] mutants, *yadH* null cells showed no change in sensitivity to lipophilic drugs (e.g., erythromycin; data not shown), or in the LPS and OMP levels (Fig. 5d), or phosphatidylethanolamine and phosphatidylglycerol phospholipid species (data not shown). Rather, the cardiolipin profile of *yadH mlaD* double mutants was altered (Fig. 5e), consistent

with the notion that Mla targets a relatively minor population of OM phospholipid molecules[44].

Cardiolipin is thought to be synthesized at the IM and transported to the OM by the IMP PbgA (YejM) in *E. coli* and other Gram-negative bacteria[45]. Consistent with this, PbgA reproducibly co-purified with MlaE in replicate AP/MS analyses, but failed to pass our stringent scoring threshold. Further experiments are required to delineate how YadH mediates selective phospholipid trafficking in conjunction with Mla/PbgA, but our data suggest a role in the maintenance of OM lipid asymmetry via selective phospholipid substrate flow (Fig. 5f).

MPC conservation and diversification

We examined the evolutionary significance of the MPCs based on their patterns of conservation, as predicted by the presence or absence of any given MPC subunit ortholog encoded in a genome[46]. Using InParanoid[47] to map orthologous relationships across bacteria (Supplementary Table 5), we observed that essential CEPs tended to be more highly conserved ($P = 4.2 \times 10^{-2}$; Supplementary Fig. 9a), even among the most highly divergent species (e.g., *Mycoplasma*, *Rickettsia*). Most (387, 68%) MPCs, however, were restricted to γ-proteobacteria (Supplementary Fig. 9a,b), which include important human pathogens (e.g., *Pseudomonas*, *Vibrio*). The degree of cePPI retention, both within and between complexes, was inversely proportional to phylogenetic distance (Fig. 2 and Supplementary Fig. 9a). For example, orthologs of subunits of the *E. coli* sulfonate-sulfur utilization (SsuEAD, Sbp) and sulfate/ thiosulfate transport (Sbp-CysP) complexes were absent in Firmicutes and Planctobacteria (Supplementary Fig. 9b), suggesting trait loss occurred in a common ancestor.

Strikingly, among the 28 putative paralogous groups (39 CEPs) in the MPC network (Supplementary Fig. 10a and Supplementary Table 5), only one-quarter (7, 25%) had interactions in common. Paralogs with shared binding partners tended to have significantly ($P = 1.6 \times 10^{-5}$) more interaction partners (Supplementary Fig. 10b), but the degree of overlap did not reflect protein sequence similarity or abundance (Supplementary Fig. 10c,d). For example, despite >80% sequence identity between the paralogs AcrB and AcrF, the former had more interactions in common with the RND-family pump MdtF, a more divergent paralog, than with the more closely related AcrF (Supplementary Fig. 10e). On the other hand, methyl-accepting chemotaxis receptors with >60% sequence similarity (Tar, Tsr, Trg, Tap) had few overlapping PPIs, possibly reflecting environmental adaptions[48]. Interactions of Trg with IMPs involved in flagellar export and motor/switch function (FliGLMN, FlhA) or basal-body assembly (FlgGI, FliF), and Tap with the cytosolic phosphatase, CheZ, controlling phosphorylated CheY binding to FliM, agree with Tap's known role in chemotaxis[2]. There were also few interactions in common seen between the OM capsule polysaccharide exporters Wza and GfcE, or the functionally related IM tyrosine protein kinases (Wzc and Etk), both with >70% sequence identity and critical roles in bacterial pathogenesis. Yet Etk co-purified with GfcE (functionally similar to Wzc/Wza), its tyrosine phosphatase partner Etp, and the predicted OM lipoprotein GfcD (Supplementary

Fig. 10e), consistent with Etk's known roles in polysaccharide secretion[49] and capsule production[50].

DISCUSSION

The physical interaction map presented here offers insights into the global functional organization of the *E. coli* CE, serving as the first biochemical blueprint of the interconnected modular architecture of this unique, conserved, and adaptive bacterial system. While we cannot exclude loss of important transient associations and disruption of hydrophobic interactions upon detergent solubilization, our systematic AP/MS approach captured thousands of known and unexpected cePPIs, revealing MPCs involved in processes central to microbial CE establishment, maintenance and integrity, and environmental responsiveness. Notably, our probabilistic network implicated previously unannotated CEPs in MP export, folding and assembly, OM biogenesis, and multidrug-resistance, examples of which we subsequently validated by independent experimentation (e.g., YadH in Mla-mediated OM lipid asymmetry maintenance). We also showed for the first time that autotransporters do not spontaneously self-assemble, but instead require chaperone assistance to nucleate folding in the periplasm before delivery to the bacterial cell surface through a cooperative mechanism involving the BAM and TAM machineries. While neither TamA nor TamB is required for passenger domain secretion, we established that BamA is the primary translocator in *E. coli*, while TamB is involved in folding and maturation.

Many additional mechanistic insights can be gleaned from the network, including CEP cross-talk critical for envelope formation and homeostasis, functional constraints underlying the evolution of Gram-negative bacteria, and potentially promising targets to potentiate existing antibiotics to combat the scourge of drug resistance. We also identified regulatory links by which HPr of the *E. coli* phosphotransferase system controls carbohydrate and energy metabolism, and unexpected associations between multiple RND-type MDR pumps, with wide-ranging relevance to bacterial pathophysiology. By making all of our data accessible via a dedicated web portal (http://ecoli.med.utoronto.ca/membrane) and public repositories (BioGRID, PRIDE accession number: PXD006247), we expect this resource will spur further exploration of other CEP complexes and interactions underlying critical CE-linked processes in other prokaryotes.

ONLINE METHODS

Topological classification of the *E. coli* proteome and target CEP selection

We have made substantial efforts to systematically re-annotate the entire collection of 4,436 putative ORFs of *E. coli* K-12 on the basis of the most current (Supplementary Table 1), carefully filtered, subcellular annotations available in respected public databases and a hand-picked set of well-regarded and widely used prediction programs (i.e., α-helical inner membrane proteins by Phobius[51], β-barrel outer membrane proteins (OMPs) by BOCTOPUS2 (ref. 52), and signal peptides intended for extracellular and periplasmic proteins by SignalP[53]), effectively supplanting questionable 'legacy' annotations.

While we do see the merit in using uniform annotations, the use of universally standardized GO terms to define topology is challenging as the GO hierarchical classifications are both very general (e.g., membrane - GO: 0016020; intracellular - GO: 0005622; cell - GO: 0005623), with distinctions such as the outer or inner lipoprotein classes largely missing. Therefore, we have compiled subcellular location information for *E. coli* K-12 proteins from six different sources: (i) our previously published *E. coli* subcellular annotation survey[6], (ii) STEPdb ver 2.0 (ref. 54), (iii) EchoLOCATION[55], (iv) EcoCyc, (v) UniProt, and (vi) GO (cellular component terms). For consistency, we list nine different subcellular compartments as broadly as possible: (i) IM, inner membrane; (ii) OM, outer membrane; (iii) PE, periplasm; (iv) LPI, IM lipoprotein; (v) LPO, OM lipoprotein; (vi) EC, extracellular; (vii) PG, peptidoglycan; (viii) MR, membrane-related; and (ix) CY, cytosol.

For each *E. coli* protein, a primary subcellular annotation was assigned based on maximum agreement (votes/counts) between these sources (referred to as “consensus” in Supplementary Table 1). In the absence of a consensus, a judgment call was made based on additional evidence such as protein function and domain information from EcoCyc as well as a manual literature search. Also, if most of the votes assigned a protein to the “no subcellular localization” category maximal, we assigned the protein to the next most likely subcellular compartment. Nevertheless, we also provide access to both the original terms provided by a given source as well as the consensus, allowing readers to view and sort annotations according to their preference.

With respect to the use of the term “membrane-associated,” we note that this assignment is used in EchoLOCATION, while UniProt refers to “membrane-related”[54]. In the “Compilation localization terms” sheet of the revised Supplementary Table 1, we have compiled annotations from the six aforementioned sources annotated as “membrane anchored,” “membrane associated,” “membrane,” “cell membrane,” “lipid anchor,” “cytoplasmic or periplasmic side of the peripheral membrane protein,” “single- and multi-pass membrane protein,” “intrinsic and extrinsic component of membrane,” “anchored component of membrane,” “cell envelope,” and “intracellular membrane-bounded organelle.” This is vital to derive meaningful information and trends regarding the membrane-related portion of the interaction network (Supplementary Figs. 2b and 5e). Nevertheless, the readers can track original annotations and curation sources.

Using this new scheme, we provide annotations documenting 1,347 putative CEPs, and during the manuscript preparation, we found an additional 270 proteins assigned to various CE categories (Supplementary Table 1) that were not purified by AP/MS. However, a significant fraction (141/270) of these proteins were detected as prey in other bait purifications, and 99 form part of our final PPI network.

Strains and plasmids

All bacterial strains, plasmids, detergents, and DNA oligonucleotides used in this study are listed in Supplementary Table 5. Primers for SPA (sequential peptide affinity)-tagging was ordered in a 96-well plate format, and transformation, integration, and western-blot verification was performed essentially as previously described[7,8,56]. While we attempted to tag 1,347 CEPs, precise recombination and perfect in-frame fusion of the SPA-tag to the

natural C terminus of the target protein was confirmed only for 785 CEPs by PCR or immunoblotting using the anti-FLAG antibody that recognizes the FLAG epitope located on SPA-tagged fusion strains[7,8,56]. Detailed detergent selection for CEP target purification and AP/MS procedures are described in Supplementary Note 1. Donor query mutant strain construction and conjugation procedures were as described[57]. The F^- recipient single-gene-deletion strains (marked with the kanamycin resistance cassette) were from the Keio knockout library[58] or the selection cassette was integrated into the 3′-UTR of essential genes to perturb transcript abundance[57]. To construct Hfr knockout mutants (marked with the chloramphenicol resistance cassette) with non-essential genes, we completely replaced the coding sequence of each open reading frame using λ-Red recombination[57].

All strains used for assaying different pump substrates were derived from *E. coli* K-12 BW-RI that constitutively produces the *tet* repressor TetR and the *lac* repressor LacI. The *acrA* and *mdtF* single mutants were purchased from the *E. coli* Genetic Stock Center. The *mdtEF* double mutant was made using the method of Datsenko and Wanner[59]. To create *acrAB* and *mdtEF* quadruple mutant (i.e., 'Quad KO Δ*acrAB mdtEF*' in Fig. 3b), the *acrAB* mutation (the substitution of a kanamycin resistance gene (Kan^r) for *acrAB*) from the previously made *acrAB* mutant TG1 *acrAB*[60] was transferred to the *mdtEF* background by P1 transduction.

To construct the *mdtEF* overexpression strain (i.e., 'Quad KO *mdtEF*$^+$' in Fig. 3b), the synthetic *tet* promoter (Ptet, a strong promoter that is repressed by TetR and the repression is released by a tetracycline or its analogs[61]) was substituted for the native *mdtEF* promoter as previously described[62]. Briefly, using the plasmid pKDT-Ptet as a template, the region ('Kan^r:*rrnB*T:Ptet') containing a Kan resistance gene (Kan^r), and an *rrnB* terminator (*rrnB*T) was amplified using the oligos Ptet.EF-P1 and Ptet.EF-P2 (Supplementary Table 5). Ptet.EF-P1 is composed of a 20-bp region at the 3′ end that is complementary to the FRT-flanking Kan^r sequence, and a 50-bp region at the 5′ end that is homologous to the upstream region of the *mdtEF* promoter. Ptet.EF-P2 is composed of a 20-bp region at the 3′ end that is complementary to Ptet, and a 50-bp region at the 5′ end that is homologous to the first 50 bp of the *mdtE* gene. The PCR products (i.e., Kan^r:*rrnB*T:Ptet) were purified and then electroporated into BW-RI *acrAB* cells, expressing the λ Red proteins encoded by plasmid pKD46. The cells were applied onto Luria–Bertani (LB) + Kan plates. Kan^r colonies were screened for the replacement of native *mdtEF* promoter (−326 to −1 relative to the start codon of *mdtE*) by the 'Kan^r:*rrnB*T:Ptet' fragment by colony PCR, followed by sequencing. The resultant strain was named 'Quad KO *mdtEF*$^+$', in which *acrAB* is deleted and *mdtEF* is under the control of Ptet.

Similarly, to make the overexpression strain '*acrA*' (i.e., 'Quad KO *acrA*$^+$'), the 'Kan^r:*rrnB*T: Ptet' fragment was substituted for the native *acrAB* promoter (−78 to −1 relative to the start codon of *acrA*) in the *acrB* and *mdtEF* deletion background, whereas for the overexpression strain '*mdtF*' in Quad KO (i.e., 'Quad KO *mdtF*$^+$'), the 'Kan^r:*rrnB*T:Ptet' fragment was substituted for the native *mdtEF* promoter, *mdtE* and the *mdtE*/*mdtF* intergenic region in the *acrAB* deletion. Likewise, the '*acrA mdtF*' overexpression strain (i.e., 'Quad KO *acrA*$^+$*mdtF*$^+$') was created by transferring the 'Kan^r:*rrnB*T:Ptet-*mdtF*' from

strain 'Quad KO *mdtF*$^{+}$' into strain 'Quad KO *acrA*$^{+}$' by P1 transduction. All constructs were confirmed by PCR and DNA sequencing.

Enriched CEP complexes sensitive to drugs

To determine drug hypersensitivity among the components of CEP complexes, we compiled the phenotypic fitness score $|\geq \pm 2|$ from large-scale phenomics screens[9] (focusing on 69 drugs that target specifically to cell wall, DNA synthesis, ribosome biogenesis and other cellular processes) for single-gene-deletion mutants corresponding to the CEP-encoding gene from the putative complexes predicted (Fig. 3a and Supplementary Table 5). Gene set enrichment analysis (GSEA)[63] was then employed with ranked lists containing drug-sensitive (fitness score ≤ -2) phenotypes from phenomics screens[9] using the predicted CEP complexes as gene sets. This analysis resulted in the significant enrichment ($P \leq 0.05$) for drug hypersensitivity among the components of 69 of the 420 distinct CEP complexes tested.

Phylogenetic tree construction and determination of orthologous sequences

The phylogenetic kinship of 20 different or diverse classes (Fig. 2 and Supplementary Fig. 9a,b) of bacteria were determined by retrieving the complete bacterial proteomes from the NCBI database. Proteomes compared using CVTree[64] and T-REX[65] were visualized using the corresponding phylogenetic trees. Specifically, this approach accounts for all protein sequences of an organism's proteome and counts the number of overlapping k-tuples to form a raw compositional vector with 20^{k} components. Random background frequencies were subtracted by predicting the number of k-tuples from k-1 and k-2 mers through a simple Markovian model. By setting these 'normalized' frequencies in a fixed order, a normalized 20^{k} dimensional vector for each organism was obtained. Finally, a correlation between two species was determined by calculating the projection of one normalized vector on another, from which a normalized distance between organisms could be gauged, allowing the construction of a phylogenetic tree.

Using all-versus-all BLASTP searches with the InParanoid script[66] of the respective proteomes for a given pair of bacterial species, protein sequence pairs appearing as reciprocally best-scoring BLAST hits between each species were selected as central orthologous pairs. Proteins of both species that showed such an elevated degree of homology were clustered around these central pairs, forming orthologous groups. The quality of the clustering was further assessed by a standard bootstrap procedure. We only considered the central orthologous sequence pair with a confidence level of 100% as the genuine orthologous relationship.

Ethidium bromide (EtBr) accumulation

E. coli BW-RI strains were grown overnight in 5 mL LB media from frozen stocks. About 150 μL of overnight-grown cultures were inoculated into 5 mL of fresh LB containing 0.2% glucose and 150 ng of chlorotetracycline for tetracycline promoter (P_{tet}). Strains carrying the P_{tet} promoter were grown with and without 150 ng chlorotetracycline for ~1 h at 37 °C until an OD_{600} of ~0.5 was reached. Cells were washed once in 1× PBS (phosphate buffered saline) and normalized to 0.15 for the EtBr retention assay.

The assay buffer consisted of 5 μg/mL EtBr, 0.4% glucose and 1× PBS in a volume of 1 mL. The cell suspensions were incubated for 30 min at room temperature to equilibrate EtBr that was retained inside the *E. coli* cells. Roughly 250 μL of the 1 mL suspension was aliquoted into three wells (analytical triplicates) on 96-well clear flat-bottom plates. The fluorescence readings were measured on a Tecan plate reader at 535 nm excitation and 612 nm emission. The cell suspension absorbance (600 nm) was also recorded to normalize the fluorescence signals.

Drug resistance assay

The assay was performed in triplicate on 1.5% LB agar plates with carbenicillin or levofloxacin (100 mg/ml; 100 μl) added in a central well. *E. coli* (BW-RI) wild-type or mutant strains were streaked from the central well to the plate periphery. As the drug diffuses out into the plate, a gradient of compound is created, killing more sensitive cells at lower concentrations. After incubating plates at 37 °C for at least 24 h, the relative sensitivities of the mutant strains were expressed in terms of the distance of the diffused killing zones (in mm) relative to wild type.

Phenotypic and immunoblot analyses

For assessing SDS-EDTA sensitivity, growth curve analyses were performed by inoculating the exponentially growing overnight cultures (OD_{600} ≈ 0.3–0.4) of the wild-type and single or double mutant strains into the 96-well microtiter plates containing 100 μl of LB medium in the presence or absence of SDS (0.5%) and EDTA (1.1 mM), incubated with shaking at 32 °C, and the absorbance of the culture was measured at OD_{600} using an automated Tecan Sunrise microplate reader every 15 min for 24 h.

For assessing the suppression of OM permeability defects of strains expressing multicopy *pldA*, respective mutant strains were transformed with pCA24N::*pldA*-His (marked with chloramphenicol) retrieved from ASKA overexpression library, following the protocol as previously described[67]. Sensitivity of the gene deletion mutant strains defective for OM was assayed using 6 mm filter paper disks (Sensi-Disc Susceptibility Test Discs; BD) impregnated with 5 μg of erythromycin by disk diffusion assay, essentially as described[44].

Immunoblots for the LPS or OM marker protein levels in the wild-type and mutant strains were performed according to standard methods described[10] with antisera raised against LptD, OmpA and MBP epitopes (a gift from T. Silhavy and C. Whitfield; see also **Life Sciences Reporting Summary**).

Phospholipid isolation and MS analyses

Total phospholipids from the wild-type and mutant strains were extracted using the procedure essentially as previously described[68]. Extracted lipids were analyzed by direct-infusion electrospray ionization, at a flow rate of 5 μl/min, in an IonMax API ion source coupled to LTQ Orbitrap Elite MS. The instrument was calibrated with Pierce ESI Negative Ion Calibration solution. Measurements were carried out in negative ion mode with the following experimental conditions: the ion-spray potential of 3.5 kV and all other voltages were optimized for maximum molecular ion transmission and the transfer capillary

temperature was set at 275 °C. Full-scan high-resolution mass spectra (R = 60,000 at m/z 400) were collected at a selected m/z range of 200 to 2,000 with a maximum injection time of 200 ms. Xcalibur software was used for data acquisition and processing.

Specially, we looked at the mass-to-charge ratio (m/z) of the product ions for phosphatidylethanolamine (PE) at 688.5 (corresponding to C15:0/ cyC17:0 and C16:0/ C16:1), 702.5 (C16:0/cyC17:0) and 714.5 (C18:1/C16:1 and cyC17:0/cyC17:0), as well as for phosphatidylglycerol at m/z 733.5 (corresponding to C16:0/cyC17:0) and 761 (C16:0/ cyC19:0) using the product ion information described for phospholipid species in *E. coli*[69]. Similarly, as per the literature evidence[70–72], we looked for the product ions of cardiolipin species at m/z 1360–1540.

Cloning of TamA, TamB and Ag43

The coding sequence of the predicted mature TamA protein from *E. coli* BL21 (*Ec*TamA22-577) was cloned in between the BamH1 and Xho1 endonuclease sites of modified pET26 expression plasmid, downstream of a PelB signal sequence, a 6× histidine tag and a thrombin cleavage site. A full-length and truncated TamB sequence from *E. coli* BL21 (*Ec*TamB1-1259; *Ec*TamB32-1259; *Ec*TamB32-923) was cloned between the NdeI and Xho1 endonuclease sites of the pET28 expression vector, downstream of a 6× histidine tag and a thrombin cleavage site. The Ag43 premature autotransporter was cloned from *E. coli* K-12 using a restriction-free cloning method[73] into a modified pHERD20T vector, downstream of a constitutive promoter.

Agglutination assay

To monitor the secretion of autotransporters, we designed an autotransporter-dependent agglutination assay in wild-type *tamA* and *tamB* mutant strains of *E. coli* K-12 BW25113 (ref. 58). Targeted gene deletion mutants were PCR verified to confirm the replacement of the genes with a kanamycin resistance cassette. Bacterial cells were transformed with the pHERD20T-Ag43, pAgH[74], pTngH[75] and pBAD18-YadA[76] expression vectors, and individual colonies were grown in LB media supplemented with appropriate antibiotics until the optical density at 600 nm reached between 2.5 and 2.8 arbitrary unit (AU). The culture was measured at OD_{600} using 100 µl aliquots taken 1 cm below the surface of the liquid culture at specific time intervals. All experiments were performed in triplicate originating from three separate colonies.

Flow cytometry

Surface translocation of the Ag43 passenger domain was evaluated by flow cytometry. *E. coli* K-12 BW25113 wild-type *tamA* and *tamB* mutant strains transformed with an empty vector or the pHERD20T-Ag43, pAgH, pTngH and pBAD18-YadA plasmids were grown in 5 ml LB media until the OD_{600} reached 3.0 AU. Cells were washed, pelleted, and resuspended in 1 ml PBS (1× PBS pH 7.0; 0.9 mM $MgCl_2$). Cells were washed a second time and resuspended in 200 µl PBS supplemented with mouse anti-His-tag primary antibodies (Pierce, Rockford, IL) at 1:200 dilution for 1 h at 4 °C.

Bacterial cells from the indicated samples were washed two times with the last resuspension procedure performed with 200 µl PBS containing anti-mouse IgG secondary antibody conjugated to phycoerythrin PE (Pierce, Rockford, IL) at 1:200 dilution, followed by 1 h incubation at 4 °C. The bacterial cells were then washed two times, and cells were fixed with 2% formaldehyde for 30 min at 25 °C. The fixed cells were analyzed with a FACSCalibur cytometer using 488 nm and 585 nm as the excitation and emission wavelengths, respectively. The threshold trigger was set on side scatter to eliminate background noise and only the intact cells were analyzed.

Proteinase-K shaving assay

Wild-type and *tamB* mutant *E. coli* cultures transformed with the pHERD20T His-Ag43 expression vector were resuspended in PBS buffer supplemented with 1 mM $MgCl_2$, 0.8 M Urea and incubated at 37 °C in the presence or absence of 0.1 mg/ml proteinase-K. About 500 µL aliquots were removed at various time points and proteinase-K was inactivated by the addition of 5 mM phenylmethanesulfonylfluoride. To insure that all clipped peptides from surface protein substrates were released in the extracellular medium, the aliquots were incubated at 55 °C for 3 min. The cells were then centrifuged at 1,500*g* for 3 min and the supernatant was analyzed by immunoblotting using anti-His-tag (HIS.H8) primary antibody to detect N-terminal His-Ag43.

Electron microscopy

For cell surface immunogold labeling, overnight bacterial cultures grown in LB media were harvested, washed with 1× PBS and then blocked with PBS containing 1% bovine serum albumin (BSA) for 1 h at room temperature. The cells were then incubated with mouse anti-His-tag (HIS.H8) primary antibody at a 1:20 dilution in PBS containing 1% BSA at 4 °C overnight. Cells were washed thrice with PBS and then blocked with PBS containing 1% BSA for 1 h at room temperature. The cells were labeled with 10 nm colloidal gold-conjugated goat anti-mouse IgG (H+L chain) at 1:20 dilution in PBS containing 1% BSA for 1 h at room temperature. Labeled cells were washed thrice with PBS followed by distilled water. Cells resuspended in distilled water were adsorbed onto formavar/carbon-coated nickel grids and stained with 1% uranyl acetate for 20 s. Air-dried grids were examined under a Hitachi H-7000 transmission electron microscope at 100 kV.

Genetic screen

The query mutant donor strains, *tamA* and *tamB*, in Hfr Cavalli (marked with chloramphenicol resistance) were screened against an arrayed select set of F^- recipient non-essential and hypomorphic alleles of essential genes using our established conjugation-based synthetic genetic array screening procedure[57].

Source code availability

Code for scoring PPIs are provided in Supplementary Note 1.

Life Sciences Reporting Summary

Further information on experimental design is available in the Life Sciences Reporting Summary.

Data availability

The PPI data from AP/MS experiments have been deposited to the ProteomeXchange Consortium via PRIDE (data set identifier: PXD006247) partner repository. The high-confidence PPIs can be accessed via our publically available web portal (http://ecoli.med.utoronto.ca/membrane) or from the open access BioGRID database dedicated to archiving PPIs for humans or model organisms. All other data are available from corresponding authors upon request.

Supplementary Material

Refer to Web version on PubMed Central for supplementary material.

Acknowledgments

We thank T. Silhavy, C. Whitfield, J.P. Côté, M. Mourez and P. Dersch for generously providing plasmids and reagents. We are also grateful to R. Reithmeier and M. Jessulat (Babu Lab) for advice. This work was supported by grants from the Canadian Institutes of Health Research to J.F.G., J.P. and A.E. (MOP-106449), J.P., A.E. and M.B. (PJT -148831) and T.F.M. (MOP-115182); the Ontario Ministry of Education and Innovation to T.F.M. and A.E.; the National Institutes of Health to P.U., M.H.S. and A.E. (GM109895); the Natural Sciences and Engineering Research Council of Canada to T.F.M. (DG-40197), A.Go. (DG-315735), J.P. (DG-06664), and M.B. (DG-20234); and the Canada Foundation for Innovation to T.F.M., M.B. and A.E.

References

1. Babu M, et al. Interaction landscape of membrane-protein complexes in *Saccharomyces cerevisiae*. Nature. 2012; 489:585–589. [PubMed: 22940862]
2. Typas A, Sourjik V. Bacterial protein networks: properties and functions. Nat Rev Microbiol. 2015; 13:559–572. [PubMed: 26256789]
3. Hurdle JG, O'Neill AJ, Chopra I, Lee RE. Targeting bacterial membrane function: an underexploited mechanism for treating persistent infections. Nat Rev Microbiol. 2011; 9:62–75. [PubMed: 21164535]
4. Hagan CL, Silhavy TJ, Kahne D. β-Barrel membrane protein assembly by the Bam complex. Annu Rev Biochem. 2011; 80:189–210. [PubMed: 21370981]
5. Whitfield C, Trent MS. Biosynthesis and export of bacterial lipopolysaccharides. Annu Rev Biochem. 2014; 83:99–128. [PubMed: 24580642]
6. Díaz-Mejía JJ, Babu M, Emili A. Computational and experimental approaches to chart the *Escherichia coli* cell-envelope-associated proteome and interactome. FEMS Microbiol Rev. 2009; 33:66–97. [PubMed: 19054114]
7. Butland G, et al. Interaction network containing conserved and essential protein complexes in *Escherichia coli*. Nature. 2005; 433:531–537. [PubMed: 15690043]
8. Hu P, et al. Global functional atlas of *Escherichia coli* encompassing previously uncharacterized proteins. PLoS Biol. 2009; 7:e96. [PubMed: 19402753]
9. Nichols RJ, et al. Phenotypic landscape of a bacterial cell. Cell. 2011; 144:143–156. [PubMed: 21185072]
10. Babu M, et al. Genetic interaction maps in *Escherichia coli* reveal functional crosstalk among cell envelope biogenesis pathways. PLoS Genet. 2011; 7:e1002377. [PubMed: 22125496]

11. Armean IM, Lilley KS, Trotter MW. Popular computational methods to assess multiprotein complexes derived from label-free affinity purification and mass spectrometry (AP-MS) experiments. Mol Cell Proteomics. 2013; 12:1–13. [PubMed: 23071097]
12. Varjosalo M, et al. Interlaboratory reproducibility of large-scale human protein-complex analysis by standardized AP-MS. Nat Methods. 2013; 10:307–314. [PubMed: 23455922]
13. Kim S, Pevzner PAMS-GF. MS-GF+ makes progress towards a universal database search tool for proteomics. Nat Commun. 2014; 5:5277. [PubMed: 25358478]
14. Lee I, Date SV, Adai AT, Marcotte EM. A probabilistic functional network of yeast genes. Science. 2004; 306:1555–1558. [PubMed: 15567862]
15. Sowa ME, Bennett EJ, Gygi SP, Harper JW. Defining the human deubiquitinating enzyme interaction landscape. Cell. 2009; 138:389–403. [PubMed: 19615732]
16. Guruharsha KG, et al. A protein complex network of *Drosophila melanogaster*. Cell. 2011; 147:690–703. [PubMed: 22036573]
17. Orchard S, et al. The MIntAct project--IntAct as a common curation platform for 11 molecular interaction databases. Nucleic Acids Res. 2014; 42:D358–D363. [PubMed: 24234451]
18. Arifuzzaman M, et al. Large-scale identification of protein-protein interaction of *Escherichia coli* K-12. Genome Res. 2006; 16:686–691. [PubMed: 16606699]
19. Rajagopala SV, et al. The binary protein-protein interaction landscape of *Escherichia coli*. Nat Biotechnol. 2014; 32:285–290. [PubMed: 24561554]
20. Szklarczyk D, et al. STRING v10: protein-protein interaction networks, integrated over the tree of life. Nucleic Acids Res. 2015; 43:D447–D452. [PubMed: 25352553]
21. Vlasblom J, et al. Novel function discovery with GeneMANIA: a new integrated resource for gene function prediction in *Escherichia coli*. Bioinformatics. 2015; 31:306–310. [PubMed: 25316676]
22. Rodionova IA, et al. The phosphocarrier protein HPr of the bacterial phosphotransferase system globally regulates energy metabolism by directly interacting with multiple enzymes in *Escherichia coli*. J Biol Chem. 2017; 292:14250–14257. [PubMed: 28634232]
23. Wang JZ, Du Z, Payattakool R, Yu PS, Chen CF. A new method to measure the semantic similarity of GO terms. Bioinformatics. 2007; 23:1274–1281. [PubMed: 17344234]
24. Babu M, et al. Quantitative genome-wide genetic interaction screens reveal global epistatic relationships of protein complexes in *Escherichia coli*. PLoS Genet. 2014; 10:e1004120. [PubMed: 24586182]
25. Kumar A, et al. Conditional epistatic interaction maps reveal global functional rewiring of genome integrity pathways in *Escherichia coli*. Cell Reports. 2016; 14:648–661. [PubMed: 26774489]
26. Wan C, et al. Panorama of ancient metazoan macromolecular complexes. Nature. 2015; 525:339–344. [PubMed: 26344197]
27. Havugimana PC, et al. A census of human soluble protein complexes. Cell. 2012; 150:1068–1081. [PubMed: 22939629]
28. Mogk A, Huber D, Bukau B. Integrating protein homeostasis strategies in prokaryotes. Cold Spring Harb Perspect Biol. 2011; 3:a004366. [PubMed: 21441580]
29. Pinske C, et al. Physiology and bioenergetics of [NiFe]-hydrogenase 2-catalyzed H2-consuming and H2-producing reactions in *Escherichia coli*. J Bacteriol. 2015; 197:296–306. [PubMed: 25368299]
30. Wang Y, et al. A supercomplex spanning the inner and outer membranes mediates the biogenesis of β-barrel outer membrane proteins in bacteria. J Biol Chem. 2016; 291:16720–16729. [PubMed: 27298319]
31. Leung HC, Xiang Q, Yiu SM, Chin FY. Predicting protein complexes from PPI data: a core-attachment approach. J Comput Biol. 2009; 16:133–144. [PubMed: 19193141]
32. Moraes TF, Reithmeier RA. Membrane transport metabolons. Biochim Biophys Acta. 2012; 1818:2687–2706. [PubMed: 22705263]
33. Charbit A, Reizer J, Saier MH Jr. Function of the duplicated IIB domain and oligomeric structure of the fructose permease of *Escherichia coli*. J Biol Chem. 1996; 271:9997–10003. [PubMed: 8626640]

34. Kim HM, Park YH, Yoon CK, Seok YJ. Histidine phosphocarrier protein regulates pyruvate kinase A activity in response to glucose in Vibrio vulnificus. Mol Microbiol. 2015; 96:293–305. [PubMed: 25598011]
35. Létoffé S, Delepelaire P, Wandersman C. The housekeeping dipeptide permease is the *Escherichia coli* heme transporter and functions with two optional peptide binding proteins. Proc Natl Acad Sci USA. 2006; 103:12891–12896. [PubMed: 16905647]
36. Petrarca P, Ammendola S, Pasquali P, Battistoni A. The Zur-regulated ZinT protein is an auxiliary component of the high-affinity ZnuABC zinc transporter that facilitates metal recruitment during severe zinc shortage. J Bacteriol. 2010; 192:1553–1564. [PubMed: 20097857]
37. Pandey R, et al. MntR(Rv2788): a transcriptional regulator that controls manganese homeostasis in Mycobacterium tuberculosis. Mol Microbiol. 2015; 98:1168–1183. [PubMed: 26337157]
38. Horazdovsky BF, Hogg RW. Genetic reconstitution of the high-affinity L-arabinose transport system. J Bacteriol. 1989; 171:3053–3059. [PubMed: 2656640]
39. Brown ED, Wright GD. Antibacterial drug discovery in the resistance era. Nature. 2016; 529:336–343. [PubMed: 26791724]
40. Selkrig J, et al. Discovery of an archetypal protein transport system in bacterial outer membranes. Nat Struct Mol Biol. 2012; 19:506–510. S1. [PubMed: 22466966]
41. Gruss F, et al. The structural basis of autotransporter translocation by TamA. Nat Struct Mol Biol. 2013; 20:1318–1320. [PubMed: 24056943]
42. Heinz E, Selkrig J, Belousoff MJ, Lithgow T. Evolution of the Translocation and Assembly Module (TAM). Genome Biol Evol. 2015; 7:1628–1643. [PubMed: 25994932]
43. Henderson IR, Owen P. The major phase-variable outer membrane protein of *Escherichia coli* structurally resembles the immunoglobulin A1 protease class of exported protein and is regulated by a novel mechanism involving Dam and oxyR. J Bacteriol. 1999; 181:2132–2141. [PubMed: 10094691]
44. Malinverni JC, Silhavy TJ. An ABC transport system that maintains lipid asymmetry in the gram-negative outer membrane. Proc Natl Acad Sci USA. 2009; 106:8009–8014. [PubMed: 19383799]
45. Dong H, et al. Structural insights into cardiolipin transfer from the Inner membrane to the outer membrane by PbgA in Gram-negative bacteria. Sci Rep. 2016; 6:30815. [PubMed: 27487745]
46. Caufield JH, Abreu M, Wimble C, Uetz P. Protein complexes in bacteria. PLOS Comput Biol. 2015; 11:e1004107. [PubMed: 25723151]
47. Ostlund G, et al. InParanoid 7: new algorithms and tools for eukaryotic orthology analysis. Nucleic Acids Res. 2010; 38:D196–D203. [PubMed: 19892828]
48. Lan G, Schulmeister S, Sourjik V, Tu Y. Adapt locally and act globally: strategy to maintain high chemoreceptor sensitivity in complex environments. Mol Syst Biol. 2011; 7:475. [PubMed: 21407212]
49. Cuthbertson L, Mainprize IL, Naismith JH, Whitfield C. Pivotal roles of the outer membrane polysaccharide export and polysaccharide copolymerase protein families in export of extracellular polysaccharides in gram-negative bacteria. Microbiol Mol Biol Rev. 2009; 73:155–177. [PubMed: 19258536]
50. Nadler C, et al. Cycling of Etk and Etp phosphorylation states is involved in formation of group 4 capsule by *Escherichia coli*. PLoS One. 2012; 7:e37984. [PubMed: 22675501]
51. Käll L, Krogh A, Sonnhammer EL. A combined transmembrane topology and signal peptide prediction method. J Mol Biol. 2004; 338:1027–1036. [PubMed: 15111065]
52. Hayat S, Peters C, Shu N, Tsirigos KD, Elofsson A. Inclusion of dyad-repeat pattern improves topology prediction of transmembrane β-barrel proteins. Bioinformatics. 2016; 32:1571–1573. [PubMed: 26794316]
53. Petersen TN, Brunak S, von Heijne G, Nielsen H. SignalP 4.0: discriminating signal peptides from transmembrane regions. Nat Methods. 2011; 8:785–786. [PubMed: 21959131]
54. Orfanoudaki G, Economou A. Proteome-wide subcellular topologies of *E. coli* polypeptides database (STEPdb). Mol Cell Proteomics. 2014; 13:3674–3687. [PubMed: 25210196]
55. Horler RS, Butcher A, Papangelopoulos N, Ashton PD, Thomas GH. EchoLOCATION: an in silico analysis of the subcellular locations of *Escherichia coli* proteins and comparison with experimentally derived locations. Bioinformatics. 2009; 25:163–166. [PubMed: 19015139]

56. Babu M, et al. Sequential peptide affinity purification system for the systematic isolation and identification of protein complexes from *Escherichia coli*. Methods Mol Biol. 2009; 564:373–400. [PubMed: 19544035]
57. Butland G, et al. eSGA: *E. coli* synthetic genetic array analysis. Nat Methods. 2008; 5:789–795. [PubMed: 18677321]
58. Baba T, et al. Construction of *Escherichia coli* K-12 in-frame, single-gene knockout mutants: the Keio collection. Mol Syst Biol. 2006; 2:0008. [PubMed: 16738554]
59. Datsenko KA, Wanner BL. One-step inactivation of chromosomal genes in *Escherichia coli* K-12 using PCR products. Proc Natl Acad Sci USA. 2000; 97:6640–6645. [PubMed: 10829079]
60. Zhang Z, et al. Functional characterization of the heterooligomeric EbrAB multidrug efflux transporter of *Bacillus subtilis*. Biochemistry. 2007; 46:5218–5225. [PubMed: 17417881]
61. Lutz R, Bujard H. Independent and tight regulation of transcriptional units in *Escherichia coli* via the LacR/O, the TetR/O and AraC/I1-I2 regulatory elements. Nucleic Acids Res. 1997; 25:1203–1210. [PubMed: 9092630]
62. Klumpp S, Zhang Z, Hwa T. Growth rate-dependent global effects on gene expression in bacteria. Cell. 2009; 139:1366–1375. [PubMed: 20064380]
63. Subramanian A, et al. Gene set enrichment analysis: a knowledge-based approach for interpreting genome-wide expression profiles. Proc Natl Acad Sci USA. 2005; 102:15545–15550. [PubMed: 16199517]
64. Xu Z, Hao B. CVTree update: a newly designed phylogenetic study platform using composition vectors and whole genomes. Nucleic Acids Res. 2009; 37:W174–W178. [PubMed: 19398429]
65. Boc A, Diallo AB, Makarenkov V. T-REX: a web server for inferring, validating and visualizing phylogenetic trees and networks. Nucleic Acids Res. 2012; 40:W573–W579. [PubMed: 22675075]
66. Remm M, Storm CE, Sonnhammer EL. Automatic clustering of orthologs and in-paralogs from pairwise species comparisons. J Mol Biol. 2001; 314:1041–1052. [PubMed: 11743721]
67. Kitagawa M, et al. Complete set of ORF clones of *Escherichia coli* ASKA library (a complete set of *E. coli* K-12 ORF archive): unique resources for biological research. DNA Res. 2005; 12:291–299. [PubMed: 16769691]
68. Bligh EG, Dyer WJ. A rapid method of total lipid extraction and purification. Can J Biochem Physiol. 1959; 37:911–917. [PubMed: 13671378]
69. Oursel D, et al. Lipid composition of membranes of *Escherichia coli* by liquid chromatography/tandem mass spectrometry using negative electrospray ionization. Rapid Commun Mass Spectrom. 2007; 21:1721–1728. [PubMed: 17477452]
70. Garrett TA, O'Neill AC, Hopson ML. Quantification of cardiolipin molecular species in *Escherichia coli* lipid extracts using liquid chromatography/electrospray ionization mass spectrometry. Rapid Commun Mass Spectrom. 2012; 26:2267–2274. [PubMed: 22956318]
71. Tyurina YY, et al. Characterization of cardiolipins and their oxidation products by LC-MS analysis. Chem Phys Lipids. 2014; 179:3–10. [PubMed: 24333544]
72. Hsu FF, Turk J. Characterization of cardiolipin as the sodiated ions by positive-ion electrospray ionization with multiple stage quadrupole ion-trap mass spectrometry. J Am Soc Mass Spectrom. 2006; 17:1146–1157. [PubMed: 16750386]
73. van den Ent F, Löwe J. RF cloning: a restriction-free method for inserting target genes into plasmids. J Biochem Biophys Methods. 2006; 67:67–74. [PubMed: 16480772]
74. Charbonneau ME, Berthiaume F, Mourez M. Proteolytic processing is not essential for multiple functions of the *Escherichia coli* autotransporter adhesin involved in diffuse adherence (AIDA-I). J Bacteriol. 2006; 188:8504–8512. [PubMed: 17041044]
75. Côté JP, Charbonneau ME, Mourez M. Glycosylation of the *Escherichia coli* TibA self-associating autotransporter influences the conformation and the functionality of the protein. PLoS One. 2013; 8:e80739. [PubMed: 24278316]
76. Heise T, Dersch P. Identification of a domain in Yersinia virulence factor YadA that is crucial for extracellular matrix-specific cell adhesion and uptake. Proc Natl Acad Sci USA. 2006; 103:3375–3380. [PubMed: 16488979]

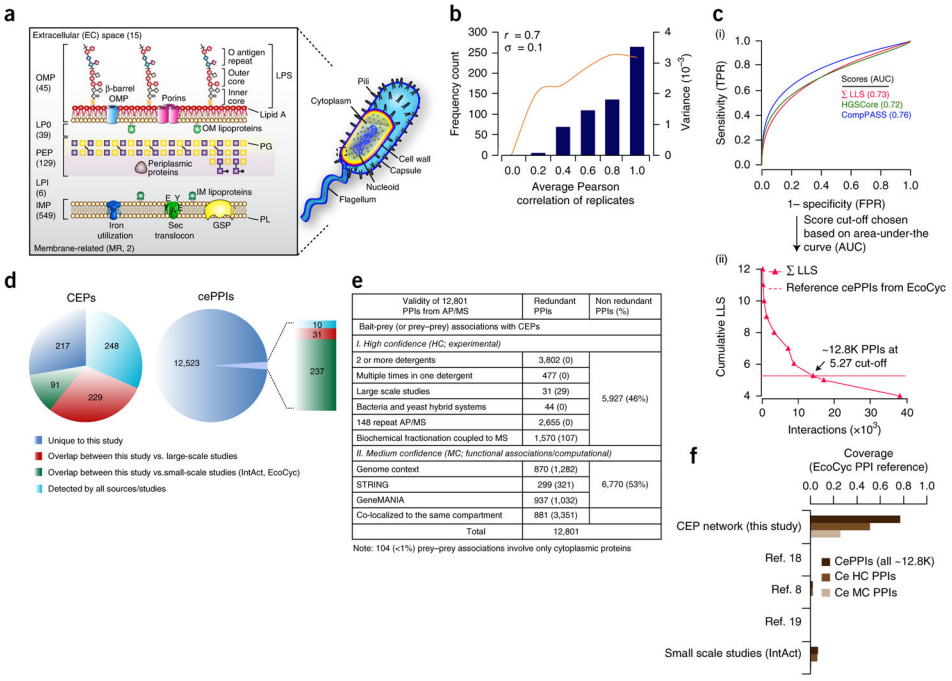

Validity of 12,801 PPIs from AP/MS	Redundant PPIs	Non redundant PPIs (%)
Bait-prey (or prey–prey) associations with CEPs		
I. High confidence (HC; experimental)		
2 or more detergents	3,802 (0)	5,927 (46%)
Multiple times in one detergent	477 (0)	
Large scale studies	31 (29)	
Bacteria and yeast hybrid systems	44 (0)	
148 repeat AP/MS	2,655 (0)	
Biochemical fractionation coupled to MS	1,570 (107)	
II. Medium confidence (MC; functional associations/computational)		
Genome context	870 (1,282)	6,770 (53%)
STRING	299 (321)	
GeneMANIA	937 (1,032)	
Co-localized to the same compartment	881 (3,351)	
Total	12,801	

Note: 104 (<1%) prey–prey associations involve only cytoplasmic proteins

Figure 1.

Purification and benchmarking of *E. coli* CEP assemblies. (**a**) Schematic of successfully tagged CEPs targeted in each envelope compartment (number in parentheses). PG, peptidoglycan; PL, phospholipid; LPI and LPO, IM- and OM-lipoproteins, respectively. (**b**) Average correlation (protein spectral counts) and variance of replicate AP/MS analyses. (**c**) Performance (true-positive rate, TPR, vs. false-positive rate, FPR) of cePPI scoring algorithms (top) and cumulative log-likelihood score (LLS; bottom). Threshold based on literature-curated interactions; Σ LLS refers to LLS HGSCore + LLS CompPASS (Supplementary Note 1). (**d**) Overlap of unique CEPs (left) and cePPIs (right) in the filtered (high + medium confidence) network compared to large[8,18,19] and small-scale (curated in IntAct or EcoCyc databases) PPI studies. (**e**) Evidence supporting AP/MS-derived cePPIs based on all available experimental, computational or functional association criteria. Number in parenthesis for redundant PPIs indicate prey-prey associations with at least one CEP. (**f**) Interaction coverage as compared to previous large[8,18,19] or small-scale studies as measured against reference cePPIs from EcoCyc.

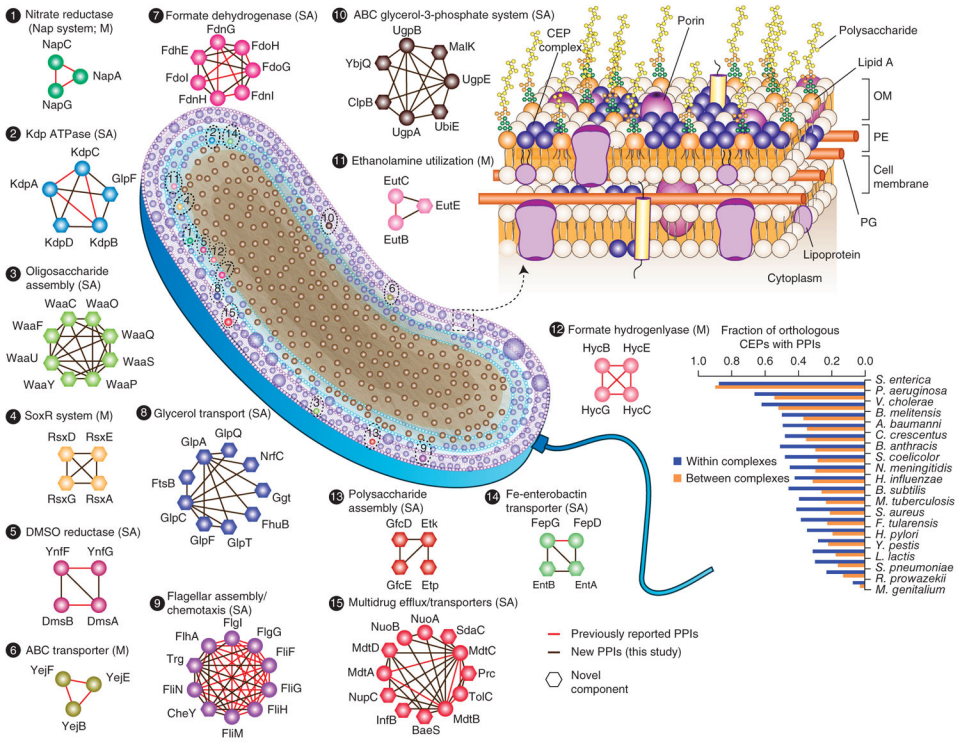

Figure 2.

Global organization and conservation of *E. coli* MPCs. Schematic showing putative *E. coli* CEP (purple circles) or cytosolic (brown circles) assemblies. CEP complex membership indicated by circle size, while edges (lines) indicate previously known (red) and novel (brown) interactions; hexagonal nodes represent putative novel components of a known complex or CE system. Topology of the MPC on the periphery indicates if the complex is based on a matrix (M) or socio-affinity (SA) model. Zoom-ins of representative highlighted complexes are shown at the periphery. Inset plot (right) shows evolutionary conservation of cePPIs based on the fraction co-occurrence of orthologs across bacterial classes for interacting CEP pairs observed within and between *E. coli* MPCs.

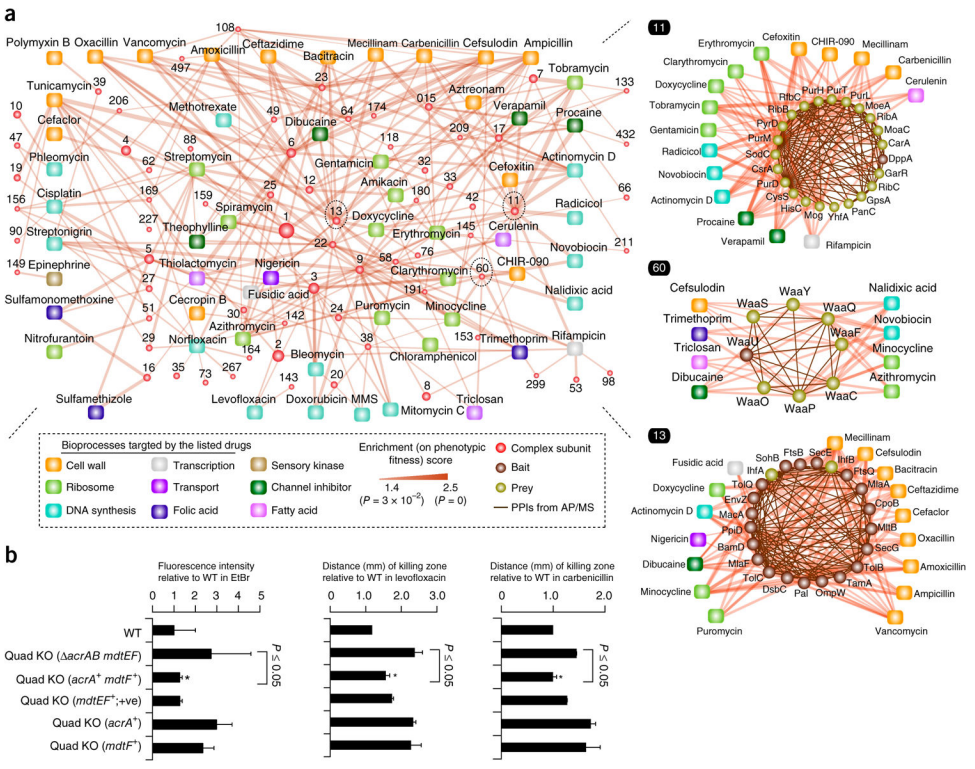

Figure 3.

CEP interactions and MPCs underlie antibiotic susceptibility. (**a**) CEP complexes conferring drug resistance[9]; node (complex ID number) size is proportional to the number of interacting components, while edge thickness is proportional to statistical enrichment (Supplementary Note 1). Zoom-in of representative complexes (dotted circles; characterized as socio-affinity model) that confer hypersensitivity to small-molecule inhibitors indicating bait (brown) and prey (green) subunits. (**b**) Graphs showing AcrA-MdtF-dependent export. Plots indicate the enhanced retention (fluorescence intensity) of ethidium bromide (EtBr, 5 μg/mL) and sensitivity (distance of the diffused killing zones) to carbenicillin or levofloxacin (100 mg/mL) of strains lacking *acrAB mdtEF* or expressing *acrA*$^{+}$ or *mdtF*$^{+}$ alone relative to *acrA*$^{+}$*mdtF*$^{+}$ or *mdtEF*$^{+}$ (+ve; positive control) together; WT, wild type; **P*-values calculated using Student's *t*-tests; error bars, mean ± s.d. from triplicate biological measurements.

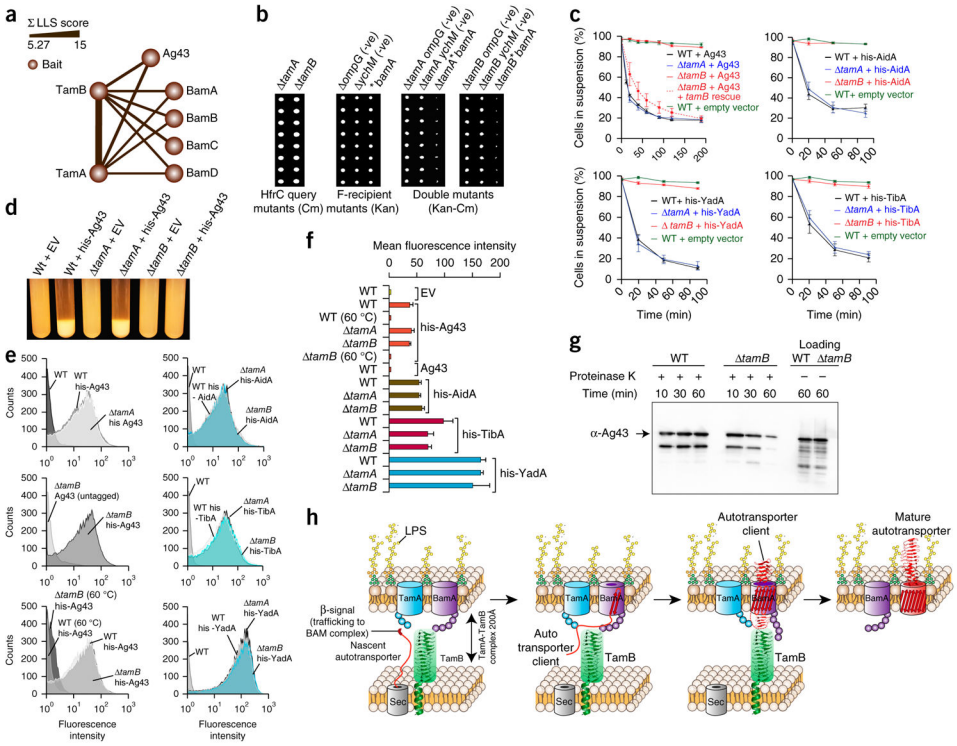

Figure 4.

Bam-Tam interconnections mediate autotransporter biogenesis. (**a**) TamA/B interacting proteins; node color indicates bait proteins involved in translocation and assembly (Tam), autotransporter (Ag43) display, and β-barrel assembly (Bam). (**b**) Synthetic growth defect of *tamA*/*B*-*bamA* double vs. single mutants and unrelated (*ompG*, *ychM*) strains; asterisk indicates hypomorphic allele. (**c**) Hyper-agglutination of *E. coli* mutants relative to wild-type (WT) cells expressing the indicated autotransporter; data represented as the mean ± s.d. from triplicate biological measurements. (**d**) Endpoint settling assay of WT and *tam* mutants expressing His-tagged Ag43 or a parental vector. (**e**) Representative flow cytometry profiles (from three biological replicates) using fluorescently labeled anti-His antibodies to quantify autotransporter passenger domain accumulation on the outer surface under normal or thermal denaturation (60 °C, 5 min) conditions; strains transformed with empty plasmid or untagged Ag43 serve as negative controls. (**f**) Export of Ag43 passenger domain, as measured by mean accumulated cell fluorescence intensity (mean ± s.d.) by flow cytometry. (**g**) Immunoblot (anti-His) time-course analysis of proteinase-K susceptibility of His-tagged Ag43 at the surface of WT cells and *tamB* mutants, along with loading controls. (**h**) Secretion model for type Va autotransporters (Supplementary Note 2).

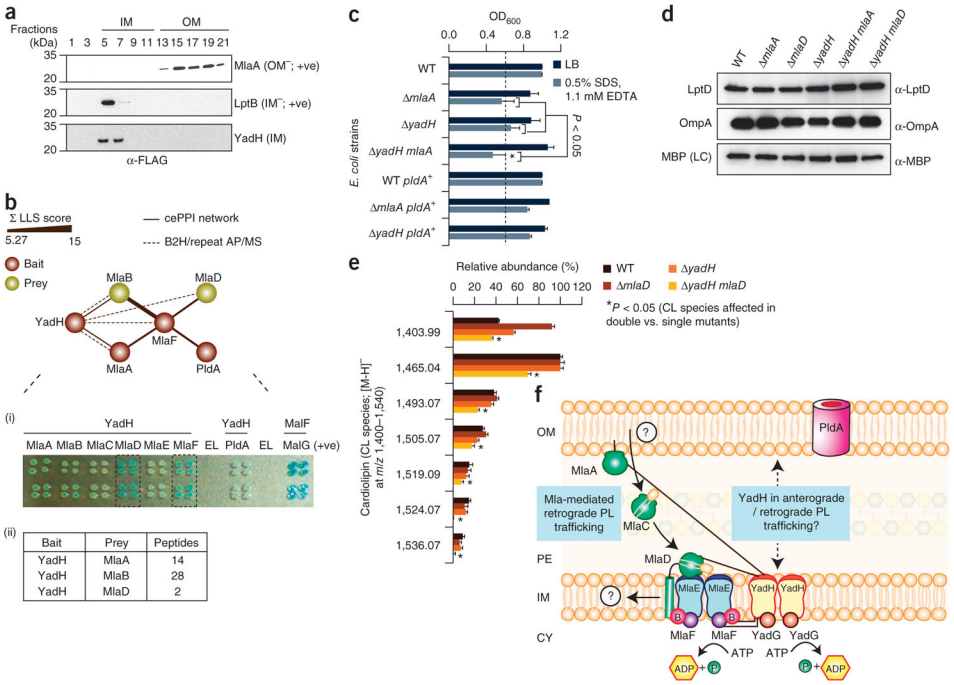

Figure 5.

YadH assists Mla-mediated phospholipid trafficking. (**a**) Immunoblot (anti-FLAG) analysis of sucrose density gradient CE fractions (lanes 1 and 3 are soluble fractions) from *E. coli* expressing FLAG-tagged YadH or controls (LptB and MlaA); molecular masses (kDa) are indicated. (**b**) YadH interactions with Mla pathway members captured by core-attachment algorithm (complex ID: 145; Supplementary Table 4); PPIs captured among Mla transporters, between Mla and surface-exposed phospholipid (PldA), or as detected by repeat AP/MS or bacterial two-hybrid (B2H) showing corresponding bait (brown) and prey (green) proteins. Zoom-in shows β-gal (i) produced by colonies (dashed boxes; EL designates empty lane). Edges (dotted lines) connecting YadH-MlaABDF reflect B2H (i) or repeat AP/MS (ii) confirmations. (**c**) Growth sensitivity (OD_{600} after 24-h culture at 32 °C) of single and double mutants vs. wild-type (WT) cells to 0.5% SDS/1.1 mM EDTA, and suppression of *yadH* hyper-permeability upon *pldA* overexpression. **P* < 0.05, by Student's *t*-test. Error bars, mean ± s.d. (**d**) Immunoblots of LPS and OMP marker levels in the indicated strains; periplasmic maltose-binding protein (MBP) serves as a loading control (LC). (**e**) Cardiolipin (CL) species quantified in single and double mutants; values indicate mean ± s.d. in ten biological replicates. **P*-value ≤ 0.05, computed using Student's *t*-test, refers to double vs. single mutants. (**f**) Model illustrating the role of YadH in Mla-mediated maintenance of OM lipid asymmetry.